Simulation of Viral Gene Delivery

Anh-Tuan Dinh[*], Theo Theofanous[**] and Samir Mitragotri[***]

[*]tuan@engr.ucsb.edu, [**]theo@engr.ucsb.edu, and [***]samir@engr.ucsb.edu
Department of Chemical Engineering
University of California, Santa Barbara, CA 93106

ABSTRACT

Here we develop an integrative computational framework to model biophysical processes involved in viral gene delivery. The model uses reaction-diffusion-advection equations that describe intracellular trafficking in combination with kinetic equations that describe transcription and translation of the exogenous DNA. It relates molecular-level microtubular binding and trafficking events to whole-cell distribution of viruses. The approach makes use of current understanding of cellular processes and data from single-particle single-cell imaging experiments. We employ the model to study the influence of microtubule-mediated movements on nuclear targeting and gene expression of adenoviruses in HeLa and A549 cells. Effects of microtubule organization and dynamics and the presence of microtubule-destabilizing drug were analyzed and quantified. Model predictions agree well with experimental data available in literature. The paper serves as a guide for future theoretical and experimental efforts to understand viral gene delivery

Keywords: adenovirus, viral gene delivery, intracellular transport, motor-assisted transport, simulation.

1 INTRODUCTION

Viruses have been used as gene delivery vehicles in a number of gene therapy studies [1]. To successfully deliver DNA into the nucleus, viruses must facilitate cell-specific binding, internalization by endocytosis, escape from endocytic vesicles into the cytosol, transport in the cytoplasm, translocation across the nuclear envelop, and finally expression of the delivered gene. A quantitative understanding of these physical processes, especially in an integrated mode, is still lacking.

Advances in fluorescence microscopy [2] have allowed researchers to follow real-time movements of viruses inside living cells at single-particle level. Useful data on intracellular transport and distribution of viruses have been obtained for various systems [3] [4].

Relatively little attention has been paid to develop quantitative models for viral gene delivery. Previous pharmacokinetic model of virus infection [5] approximated all trafficking events, including transport as kinetic processes. This yields a number of ordinary differential equations (ODEs) to describe viral concentrations in different cellular compartments. Although kinetic models can describe some aspects of viral trafficking, they lack the ability to describe spatio-temporal evolution of virus distribution. Furthermore, a number of characteristic dynamic events, such as microtubule-dependent transport are lost in this approximation. Therefore, it is of interest to develop a new modeling approach that captures the inherent cellular dynamics and predicts viral behavior that can be directly compared to data obtained from particle tracking experiments.

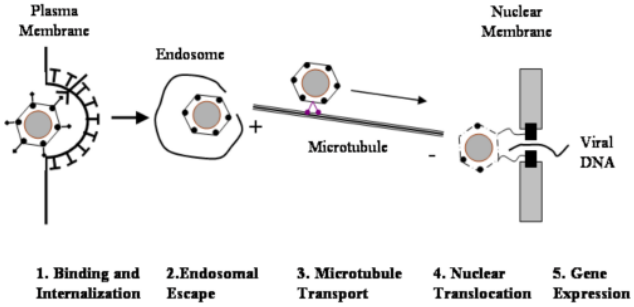

Figure 1. Gene delivery pathway of adenoviruses.

Recently, Smith and Simmons [6] developed a one-dimensional macroscopic model for motor-assisted transport of intracellular particles (vesicles, organelles, etc.) on a network of aligned filaments. These particles (complexes of vesicles and motor proteins) switch intermittently between distinct movement states, namely diffusion and directional transport on the filaments. This multi-state description of particle motion relates the kinetics of particle-filament association and dissociation to the distribution of particles along the filaments.

In the present study, we integrate the above model of motor-assisted transport with several basic features of pharmacokinetic models to describe two-dimensional intracellular trafficking of viruses. In essence, we replace the kinetic description of microtubular transport and cytosolic diffusion in earlier models of gene delivery with transport theories. Remaining steps, for example, receptor-mediated binding, internalization, endosomal escape, and nuclear translocation are described using kinetic equations. The viruses are either bound to cell membrane, caged inside endosomes, free in cytosol or bound to nuclear membrane. The viral species are defined according to these distinct biophysical states. Each species is characterized by a set of transport coefficients and a transition rate to the next state. As a result, we obtain a system of transport-reaction

equations for concentration of each viral species as a function of distance from the cell center. The equations were solved numerically using standard algorithms for partial differential equations (PDEs). This allowed us to determine the accumulation of viruses in the nuclear region. Transcription and translation of the exogenous DNA delivered by viruses were described by kinetic equations [7]. Thus, the model presented here represents a complete description of viral gene delivery at cellular level. Such models provide a platform to integrate existing experimental observations and qualitative hypotheses in a consistent manner.

2 MODEL FORMULATION

In analogy to single-particle tracking experiments, the proposed model follows the viral trajectory in a two dimensional domain. We employ a simplified two-dimensional abstraction of cells: a cell is represented by a circle of radius R_C with its nucleus occupying a circular region of radius R_N at the center. This geometry imitates a cell spread on a surface. Viruses bind to and enter the cell from the top surface. MTs grow radially from the cell center towards the cell periphery, serving as cytoskeletal tracks for viral particles.

Intracellular Trafficking: After binding to the cell membrane, the movement pathway of a viral particle can be characterized by five distinct biophysical states: membrane-bound virus (*M*), endosomal virus (*E*), cytosolic virus (*C*), nuclear-bound virus (*N*) and disassembled viral capsids (*cap*). Transition from one state to another depends on various biological and physical factors, such as location, interactions with cellular organelles, and molecular components of viral capsids. In the rest of the paper, we will refer to the biophysical states of viruses as *species*.

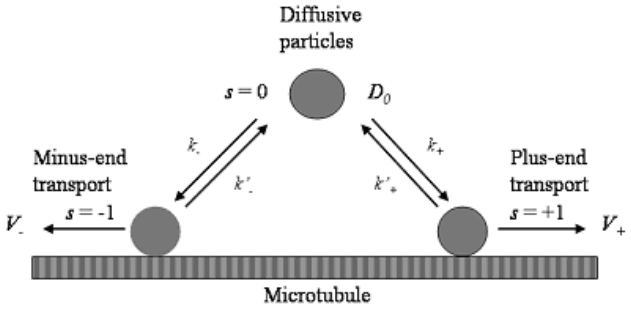

Figure 2. Transition map between transport states (0: diffusion; -1: minus-end transport; +1: plus-end transport). $k_{\pm}$ and $k'_{\pm}$ are binding/detachment rates to/from MTs. $V_{\pm}$ are the velocities of motor-assisted transport in ± directions. D_0 is coefficient for free diffusion in cytosol.

In the cytoplasmic region ($R_N < r < R_C$), a viral particle can switch intermittently between diffusion and directional transport. To account for these distinct transport processes, we introduce substate variable s, s = ±1 and 0 (0: diffusion, +1: plus-end directional transport and -1: minus-end directional transport). Transitions between transport states of viral species are illustrated in Fig. 2. In the nuclear region ($r < R_N$), the only transport state is diffusion. Since transport of viruses along the microtubules is essentially one-dimensional, a natural spatial coordinate for the problem is the distance from the cell center, r. Based on the proposed multistate description of transport, we formulate a system of macroscopic mass conservation equations for the viral species along the radial coordinate, averaging over all angles. Due to space limitation, only the equations for cytosolic viruses are given here:

a) $R_N < r < R_C$

$$\frac{\partial n_0^C}{\partial t} = (k'_{-C} n_{-1}^C + k'_{+C} n_{+1}^C) - (k_{-C} n_0^C + k_{-C} n_0^C) + D^C \frac{\partial}{\partial r}\left[r \frac{\partial}{\partial r}\left(\frac{n_0^C}{r} \right) \right]$$

$$+ k_{escape} n^E - k_{nuclear} n_0^C$$

$$\frac{\partial n_{-1}^C}{\partial t} = -k'_{-C} n_{-C}^C + k_{-C} n_0^C - V_-^C \frac{\partial n_{-1}^C}{\partial r}$$

$$\frac{\partial n_{+1}^C}{\partial t} = -k'_{+C} n_{+C}^C + k_{+C} n_0^C - V_+^C \frac{\partial n_{+1}^C}{\partial r}$$

b) $r < R_N$

$$\frac{\partial n_0^C}{\partial t} = D^C \frac{\partial}{\partial r}\left[r \frac{\partial}{\partial r}\left(\frac{n_0^C}{r} \right) \right] + k_{escape} n^E - k_{nuclear} n_0^C$$

The basic variable is the radial density $n_s^S(r,t)$ (#virus/length), which represents the number of viral particles at state *S* (*S* = *M, E, C, N* and *cap*) and substate *s* (0, -1, and +1), at distance *r* from the cell center. Note that $n_s^S(r,t)$ is not a local quantity but represents an ensemble average of particle positions with respect to the cell center, sampled over a large number of particles and a large population of cells. We choose to deal with the radial density since it conveniently captures the one-dimensional nature of transport along the MTs. Alternatively, we can formulate the equations in term of the areal density $c_s^S(r,t)$.

***2. Gene Expression*:** A reasonable assumption is that the amount of exogenous DNA entering the nucleus is proportional to the number of nuclear-bound viruses that disassemble. The equation for the evolution of exogenous DNA inside the nucleus is as follows:

$$\frac{dDNA}{dt} = \kappa_{DNA} \int_0^{R_N} k_{dissasembly} n^N dr - k_{el-DNA} DNA \qquad (3)$$

where κ_{DNA} is a proportionality constant, and $k_{el\text{-}DNA}$ is the elimination rate of exogenous DNAs by nuclease degradation and cell division.

The transcription and translation of exogenous DNA involves thousands of complex chemical reactions. In the simplest model of gene expression, mRNA is synthesized from DNA and protein is synthesized from mRNA [6]. The ordinary differential equations that determine the temporal

evolution of number of mRNA molecules, *mRNA*, and protein molecules, *P*, are

$$\frac{dmRNA}{dt} = k_{transcription} DNA - k_{deg,mRNA} mRNA \qquad (4)$$

$$\frac{dP}{dt} = k_{translation} mRNA - k_{deg,protein} P \qquad (5)$$

where $k_{trascription}$ and $k_{tranlation}$ are the transcription and translation rate constants, $k_{deg,mRNA}$ and $k_{deg,protein}$ are the decay constants associated with the half-life of mRNA and proteins.

3 RESULTS AND DISCUSSION

Spatiotemporal Distribution of Viral Particles: The model was used to simulate intracellular trafficking of adenovirus type 2 (Ad2) in HeLa cells. The simulation results are compared to the intracellular distribution data independently reported by Nakano and Greber [4]. In these experiments, the intracellular domain is divided into 4 separate areas, namely, peripheral, cytoplasmic, perinuclear and nuclear. Based on the simulated viral dynamics, we calculate the average viral density, *c*, in each area and compare with the measured fluorescence signal. Without any fitted parameters, the model predicts the experimental data with good agreement (Fig. 3).

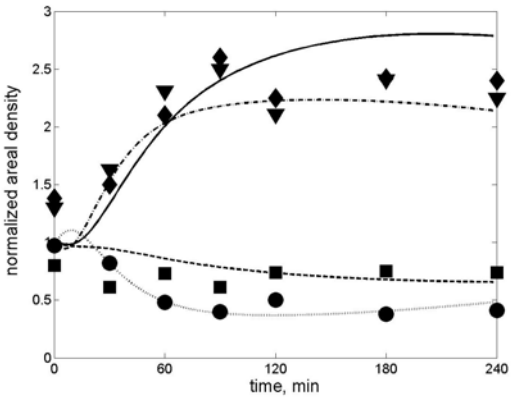

Figure 3. Distribution of Ads in HeLa cells for 4 different cellular areas: periphery (dotted line: model; circle: data), cytoplasm (dashed line: model; square: data), perinuclear (dash-dot line: model; diamond: data) and nuclear (solid line: model; triangle: data).

Apparent Transport Coefficients: Microtubules can transport Ads while they are encapsulated in endosomes and when they are released into the cytosol. However, as seen in Fig. 4, Ads only spend a brief period staying inside endosomes. Thus, at long times, intracellular allocation of viral particles is primarily determined by movements of cytosolic viruses. The directionality of these movements is measured by the effective population velocity, V_{eff}^{C}, defined as follows [8]:

$$V_{eff}^{C} = \frac{K_{+}^{C} V_{+}^{C} + K_{-}^{C} V_{-}^{C}}{K_{+}^{C} + K_{-}^{C} + 1} \qquad (7)$$

where $K_{\pm}^{C} = k_{\pm} / k_{\pm}^{/}$. Also, bidirectional random walks of cytosolic viruses on the MTs give rise to a form of facilitated diffusion along the radial coordinate. The effective diffusion coefficient that characterizes this process can be estimated by neglecting free diffusion as follows [8]:

$$D_{eff}^{C} \sim \frac{K_{+}^{C}(V_{+}^{C} - V_{eff}^{C})^2 / k_{+}^{/} + K_{-}^{C}(V_{-}^{C} - V_{eff}^{C})^2 / k_{-}^{/}}{K_{+}^{C} + K_{-}^{C} + 1} \qquad (8)$$

Thus, V_{eff}^{C} reflects the ability of particles to accumulate, whereas D_{eff}^{C} reflects the ability of particles to equilibrate along MTs. Let's consider a special case, $V_{eff}^{C} = 0$. Such unbiased bidirectional transport does not result in any net transport. However, at short time, the radial density *n(r,t)* is higher at the cell periphery, because of initial 2D random allocation of viruses. This leads to a nonequilibirium condition from a 1D perspective. Due to enhanced dispersion of particle movements, *n(r,t)* will gradually equilibrate along the radial coordinate *r*. The rate of such equilibration process is measured by D_{eff}^{C}. So even in the case of unbiased bidirectional transport ($V_{eff}^{C} \sim 0$), viruses can be efficiently delivered to the nuclear region due to the initial imbalance of viral concentration along MTs. This is quite contrary to conventional wisdoms on intracellular transport.

Cells use several mechanisms to control the activities and interactions of molecular motors in order to regulate directional movements on microtubules. There is evidence that viruses are able to utilize these mechanisms to enhance their nuclear targeting [8].. Thus, a potential antiviral strategy is to develop therapeutic agents that inhibit or impair dynein-driven transport of viruses, for instance, by interfering with binding of cytoplamic dyneins to viral capsids or suppressing signalings that enhance retrograde movements. Calculations show that such strategy can be very effective and reduces up to 90% of viral gene expression (data not shown).

Effects of Nocodazole: The frequency of directional movements on microtubules is strongly influenced by microtubule organization and polymerization dynamics. The rate at which particles bind to and get carried on a microtubule (*k*) depends on the half-life of microtubules, $t_{1/2}^{MT}$, and the average distance between two neighboring MTs, δ_{MT}. Nocodazole forms inactive complexes with tubulin dimers, reducing the free tubulin concentration. When tubulin concentration drops below a critical threshold, MTs will disassemble []. The presence of nocodazole increases the catastrophe frequency, f_{cat}, and reduces the number of stable MTs, N_{MT}. We formulate equations that relate f_{cat} and N_{MT} to nocodazole concentration [NOC]. This allows us to calculate the forward binding rates $k_{\pm}^{S}$ as function of [NOC].

The above approximation is used to analyze the effects of nocodazole on nuclear accumulation and gene expression of adenovirus in human lung carcinoma A549 cells [3]. Fig. 4 shows the model predictions of viral intracellular distribution at 75 min for a wide range of [NOC]. The simulation results capture the dose-dependent inhibitory effects of nocodazole. Evidently, high concentrations of nocodazole block transport from distal areas to nucleus. Treatment of cells with 2 μM and 20 μM NOC resulted in 50% and 60% inhibition of nuclear targeting of incoming adenoviruses, respectively.

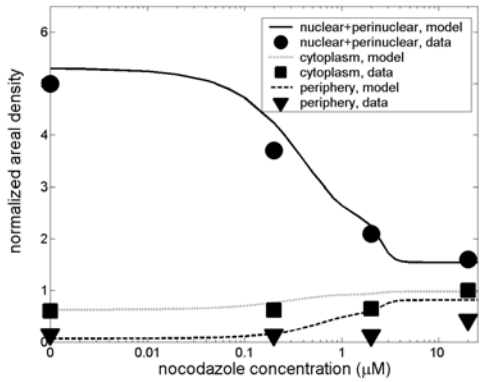

Figure 4. Normalized areal density in each cellular region at 75 min p.i. as function of nocodazole concentration. Data was reproduced from [3] for intracellular distribution of Ad2 in A549 cells.

Inhibition of microtubule-dependent transport reduces the amount of exogenous DNA delivered to the nucleus. To quantify this effect, we use the model to simulate experiments that measure β-Gal expression of Ads in A549 cells [3]. The cells contain either intact or NOC-disrupted microtubules. The predicted and measured levels of gene expression at 7h p.i. (normalized with control) are shown in Fig. 5 as function of [NOC]. Small concentrations of NOC ([NOC] < 0.4 μM) only partially destabilize the MT network and have only a slight effect on β-Gal expression. On the other hand, high concentrations of NOC ([NOC] > 10 μM) completely depolymerize the microtubule network, preventing effective viral targeting to the nucleus. Only a few viruses initially located at the nuclear region are able to bind to the nuclear membrane and release the exogenous DNA into the nucleus. This severely reduces transgene expression to merely 10-20% compared to untreated cells.

4 CONCLUSION

In the present study, we have developed a comprehensive and integrative computational framework for intracellular trafficking and gene expression of adenovirus. The numerical values of the model parameters were adapted directly from previous reports in literature. Without any fitting, the model was able to predict the measured spatiotemporal distribution of Ads in HeLa cells with reasonable agreements. We used the model to quantify the role of microtubule-transport on nuclear-targeting of viruses. Such quantitative understanding is important in developing therapeutic applications and antiviral strategies for adenovirus. With appropriate modifications, the modeling approach can be applied to other viruses, including human immunodeficiency virus (HIV) and herpes simplex virus (HSV).

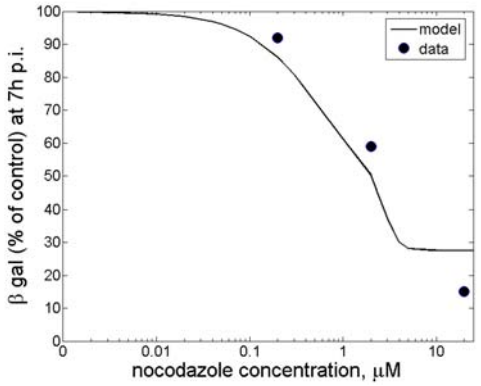

Figure 5. Viral gene expression at 7 h p.i. as a function of nocodazole concentration. Data was reproduced from [3] for Ad2-mediated expression of β-gal in A549 cells.

The real value of the model is in using transport processes (diffusion and convention) to describe important steps in viral transport. While doing so, the model makes a strong step towards realistic and physically-based description of viral dynamics. As more and more mechanistic information become available on viral dynamics, such realistic models that are applicable for a broad set of data (beyond the data used for determining model parameters) will prove valuable.

Acknowledgments

We thank Prof. Nam Dinh and Chinmay Pangakar for their helpful discussions related to the subject. A.T.Dinh is supported by U.C. Biotech Fellowship Program.

REFERENCES

[1] Verma, I.M. and N. Somia. Nature. 389:239-242., 1997.
[2] Suomalainen M., M.Y. Nakano, S. Keller, K. Boucke, R.P. Stidwill and U.F. Geber. 1999.. J. Cell Biol. 144:657-672.
[3] Mabit, H., M.Y. Nakano, U. Prank, B. Saam, K. Dohner, B. Sodeik, and U.F. Greber. 2002. J. Virology 76:9962-9971.
[4] Nakano, M.Y. and U.F. Greber. 2000.. J. Struct. Bio. 129:57-68.
[5] Dee K.U., and M.L. Shuler. 1997. Biotech Bioeng. 54:468–490.
[6] Smith, D.A., and R.M. Simmons. 2001. *Biophys. J.* 80:45-68.
[7] Kamiya, H., H. Akita, and H. Harashima. 2003. *Drug Discov. Today.* 8:990-996.
[8] Suomalainen M., M.Y. Nakano, K. Boucke, R.P. Stidwill and U.F. Geber.. 2001. EMBO J. 20:1310-1319.